Fall 8-27-2015

Strong Resistance to Bending Observed for Nanoparticle Membranes

Yifan Wang

Jianhui Liao

Sean P. McBride
Marshall University, mcbrides@marshall.edu

Efi Efrati

Xiao-Min Lin

See next page for additional authors

Recommended Citation

Wang, Y., Liao, J., McBride, S. P., Efrati, E., Lin, X. M., & Jaeger, H. M. Strong resistance to bending observed for nanoparticle membranes. Nano Lett, 2015, 15(10), 6732-6737. doi: 10.1021/acs.nanolett.5b02587

NANO LETTERS

Letter

pubs.acs.org/NanoLett

Strong Resistance to Bending Observed for Nanoparticle Membranes

Yifan Wang,[*,†,‡] Jianhui Liao,[‡,§] Sean P. McBride,[‡] Efi Efrati,[‡,∥] Xiao-Min Lin,[⊥] and Heinrich M. Jaeger[†,‡]

[†]Department of Physics, University of Chicago, 5720 S. Ellis Avenue, Chicago, Illinois 60637, United States

[‡]James Franck Institute, University of Chicago, 929 E. 57th Street, Chicago, Illinois 60637, United States

[§]Key Laboratory for the Physics and Chemistry of Nanodevices, Department of Electronics, Peking University, Beijing, 100871, China

[∥]Department of Physics of Complex Systems, Weizmann Institude of Science, Rehovot, 76100, Israel

[⊥]Center for Nanoscale Materials, Argonne National Laboratory, 9700 South Cass Avenue, Argonne, Illinois 60439, United States

Supporting Information

ABSTRACT: We demonstrate how gold nanoparticle monolayers can be curled up into hollow scrolls that make it possible to extract both bending and stretching moduli from indentation by atomic force microscopy. We find a bending modulus that is 2 orders of magnitude larger than predicted by standard continuum elasticity, an enhancement we associate with nonlocal microstructural constraints. This finding opens up new opportunities for independent control of resistance to bending and stretching at the nanoscale.

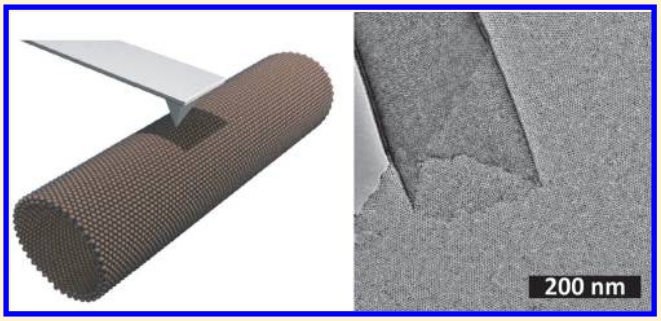

KEYWORDS: *Nanoparticle, membrane, bending, bending modulus, indentation, persistence length*

Ultrathin sheets comprised of a few layers of atoms, such as graphene,[1−3] or a few layers of close-packed, ligated nanoparticles[4−12] have attracted much interest because of their unique properties. In terms of mechanical properties, most attention has focused on nominally flat sheets. These thin sheets have been found to be mechanically robust and remarkably stiff under extension, capable of forming large freestanding membranes.[5−7,10,13−15] However, out-of-plane bending, while playing a key role in emerging fields such as the manipulation of thin films into three-dimensional structures,[9,16−19] is just starting to be explored[3] in systematic experiments for ultrathin sheets. With thicknesses on the order of or below 10 nm, such sheets are expected to be highly flexible and responsive to out-of-plane bending. The questions we are addressing here are to what extent the resistance to bending can be derived from knowledge of the physical thickness of the sheet and its tensile strength, and how one can extract the bending modulus.

In general, the resistance of a thin sheet to elastic deformation via stretching and bending is characterized by the in-plane, two-dimensional (2D) Young's modulus E_{2D} and by the out-of-plane bending modulus κ, respectively. These two parameters define an effective bending thickness t_{eff} through the relationship $\kappa = E_{2D}t_{eff}^2/12(1 - \nu^2)$, where ν is Poisson's ratio. E_{2D} is related to the bulk Young's modulus E via $E_{2D} = Et$, where t is the physical thickness of the sheet.

For homogeneous planar materials t_{eff} corresponds to the physical thickness t, but going beyond standard continuum elasticity, t_{eff} can encapsulate effects due to deviations from planarity or from the continuum limit. The former occurs, for example, when thermal or quenched height fluctuations increase the resistance to bending and thus the effective thickness,[3,20] similar to what happens in a crumpled sheet of paper, while the latter can occur when the physical thickness becomes close to the size of the constituent particles so that particle-scale features and any resulting (nonlocal) structural constraints need to be accounted for.[21−25] In either case, the experimental problem is that E_{2D} (or E) and κ are not simply related by the physical thickness t and thus need to be measured independently. This typically requires two distinct types of measurements probing separately the different modes of deformation in isolation.

Here we introduce an approach that circumvents this difficulty. As is the case for a thin, floppy sheet of paper, rolling up a monolayer into a hollow tube turns it into a stiffer and thus more easily probed structure. Importantly, the tube's response to small local indentations is a signature of contributions from both bending and stretching. As a result, a single set of measurements of the resistance to indentation along the length of a tube provides direct access to E_{2D} as well as κ.

There are several ways to bend freestanding nanoparticle sheets into tube-like structures. One is via exposure to an electron beam. Our previous work used electron-beam exposure to roll up freestanding monolayers into scrolls.[26,27] However, the e-beam also cross-links the ligands and changes

Received: June 30, 2015
Revised: August 24, 2015
Published: August 27, 2015

DOI: 10.1021/acs.nanolett.5b02587
Nano Lett. 2015, 15, 6732−6737

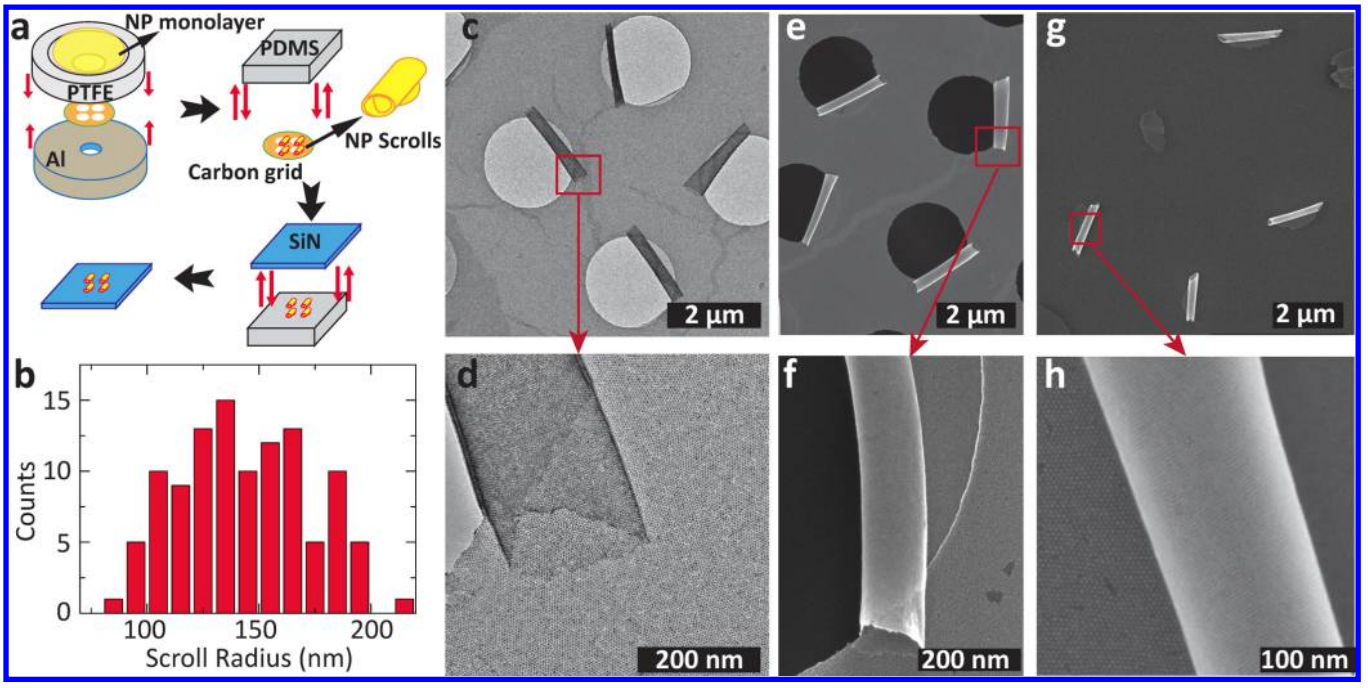

Figure 1. Self-assembly and transfer of nanoparticle scrolls. (a) Schematic of fabrication steps. Nanoparticle monolayers are assembled at the air−water interface in a PTFE holder and dried onto a carbon TEM grid containing 2 μm diameter holes placed at the bottom of the holder. Right after the water dewets the carbon grid, weak nanoparticle membranes partially detach from the holes' rims and spontaneously roll up. By gently contacting the scrolls with a PDMS stamp, they can be pulled off the carbon grids and transferred to Si/SiN wafers that have been coated with dodecyltrichlorosilane. Due to stronger adhesion to the silane than to the PDMS, the scrolls stick to the wafer. (b) Histogram of the scroll radius distribution. The radius R is determined by the strain gradient across the monolayer prior to curling up. From the average $R \approx 150$ nm, we estimate an initial strain difference $\Delta\varepsilon = (t_0/R) \approx 5\%$ between the two sides of a monolayer. This is based on an average monolayer thickness $t_0 = 7$ nm, as obtained from AFM measurements on multilayers of the same particles but deposited on flat surfaces.[15] (c, d) TEM images of free-standing nanoparticle scrolls on a holey carbon grid. Individual nanoparticles with ≈5.2 nm diameter can be resolved. Due to the circular shape of the original monolayer piece that curled up, the wall thickness increases toward the scroll center, and the portions extending beyond the hole remain the thinnest. (e, f) SEM images of nanoparticle scrolls on a holey carbon grid. (g, h) SEM image of nanoparticle scrolls after transfer.

the mechanical properties.[14] In the experiments discussed here, an alternative, noninvasive method is used, whereby nanoparticle monolayers curl up spontaneously (Figure 1).

Dodecanethiol ligand-capped gold nanoparticles with diameters of (5.2 ± 0.3) nm, suspended in toluene, were synthesized using a digestive ripening method.[28] Monolayers were assembled by adding 8 μL of nanoparticle solution onto a 100 μL distilled water droplet deposited in a cone-shaped PTFE holder (Figure 1a, alternative droplet drying methods[13] can also be used create scrolls under appropriate thiol conditions). A carbon grid (Quantifoil 657-200-CU from Ted Pella) with 2 μm diameter circular holes was clamped between the PTFE holder and an aluminum disk, and the nanoparticle monolayer eventually deposits onto the carbon grid after the water droplet evaporated. The mechanical strength of the resulting freestanding sheets inside the holes was adjusted by carefully tuning the ligand concentration in the solvent such that they tended to detach along one side of a hole as the last remaining water evaporated underneath. Partially detached monolayers spontaneously rolled up toward the air-facing side (the opposite direction of previously observed electron beam induced folding),[26,27] resulting in multilayered nanoparticle scrolls, as imaged by a JEOL JEM-2100F transmission electron microscope (Figure 1c,d) and a FEI Nova NanoLab SEM (Figure 1e,f). We believe this curling is driven by residual water trapped preferentially in the ligands of the originally water-facing side of the monolayers: water has a larger modulus than the alkanethiol ligands, and thus the bottom side of a monolayer in contact with water relaxes less when the membrane detaches and its draping-induced prestrain is released. This is supported by the fact that spontaneous curling did not occur when monolayers detached (or were strain relieved by ion beam cutting)[27] after having fully dried.

Polydimethylsiloxane (PDMS) stamps were used to transfer the scrolls from the carbon grids to SiN/Si substrates (Si coated with 50−100 nm of SiN). The substrate surfaces were modified by coating them with dodecyltrichlorosilane (Sigma-Aldrich) to enhance sticking of the scrolls after transfer. The PDMS stamps were made by mixing the base and curing agent (SYLGARD 184 Silicone Elastomer Kit, Fisher Scientific) with a ratio of 7:1, followed by degassing and curing at 70 °C for 1 h. Since the elastic modulus of the nanoparticle scrolls exceeds that of PDMS by more than a factor of a thousand,[5,13,15] most of the deformation during stamping took place inside the PDMS, and the scrolls showed no evidence of crumpling, collapse, or other irreversible plastic deformation. However, we found that the pressure from the PDMS stamp shears off the single-layered sections that extend over the hole at both ends of a scroll (the ends are necessarily single-layered because the scrolls form by rolling up circular sheets; Figure 1c−f). Therefore, only the central, multilayered part of the scrolls was transferred onto the wafer (see Supporting Information Figures S1 and S2). The radii R of over 100 measured scrolls ranged from 50 to 250 nm, with mean ∼150 nm, as determined by SEM (Figure 1g,h). Given 2 μm diameter circular sheets as starting material, this

DOI: 10.1021/acs.nanolett.5b02587
Nano Lett. 2015, 15, 6732−6737

implies a final scroll wall thickness of 2−3 monolayers (see Supporting Information Figures S1 and S2).

Figure 2 shows examples of nanoparticle scrolls imaged and indented by an Asylum MFP3D atomic force microscope

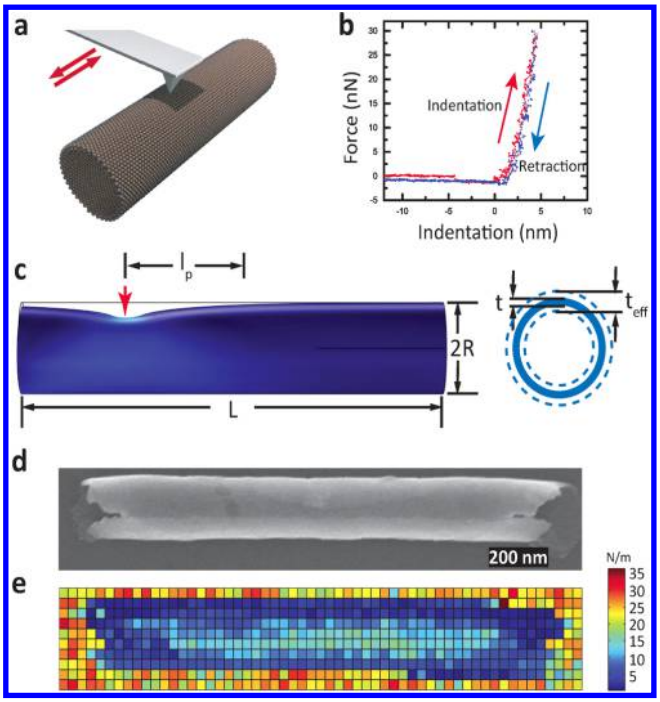

Figure 2. Indentation stiffness maps. (a) Illustration of an AFM cantilever tip scanning and indenting a nanoparticle scroll. (b) Typical force−indentation curve taken at the center of a scroll. (c) Sketch of a tube deformed after indentation (left) and its cross section. The side view on the left is obtained from a COMSOL simulation of a thick tube indented at the red arrow. The parameters l_p, R, and L are identified. The cross section on the right shows the physical thickness t and effective thickness t_{eff} for bending. (d) SEM image of a nanoparticle scroll (radius R = 90 nm, length L = 1.7 μm). (e) Stiffness map of the scroll in d. To obtain the stiffness map, the MFP3D AFM was programmed to indent at a grid of points within a selected rectangular area above a scroll's central axis. The indentation targets were spaced ≈37 nm both in the axial, x-direction and the transverse, y-direction, resulting in a force−indentation map of 57 × 10 pixels over a 2.1 × 0.37 μm area. The stiffness values at each point were calculated from a linear fit to the indentation approach data, using a Matlab script. Note that along the direction transverse to the central x-axis, the decrease of stiffness to either side of the scroll apex is caused by some slip of the AFM tip when the tip trajectory is not perpendicular to the scroll surface. Therefore, only values within close proximity of the x-axis were used for analysis. Note also the larger stiffness along the top ridge of the scroll and the drop-off near the open ends. The AppNano ACTA cantilevers used here have a measured resonance frequency of ∼300 kHz and a spring constant of 14−20 N/m, which matches the stiffness of the scrolls. The orange/red colors reflect the larger stiffness of the substrate (given our particular AFM cantilever, with its stiffness appropriately matched to that of the scroll, those values are beyond the range of reliable measurement).

(AFM) equipped with AppNano ACTA cantilevers. In all cases, the maximun indentation applied was <10 nm, which is below the wall thickness of the scroll, to avoid buckling.[29,30] Using AFM, we found that height variations along the longitudinal direction of scroll surface stayed within 5 nm, bounding the magnitude of possible stiffening due to quenched or thermal shape fluctuations. This differs from recent findings of several thousand times bending modulus enhancement in monolayer graphene, where very strong stiffening was associated with large, ∼100 nm ripples.[3] The indentation curves were essentially linear, with little hysteresis between indentation and retraction, implying the deformation was small enough to stay in the linear elastic regime. The local stiffness k, i.e., the local effective spring constant, was calculated from the slope of force curves as in Figure 2b, and a stiffness map was obtained.

The resulting map (Figure 2e) exhibits several important features. First, the stiffness values, ranging from 10−30 N/m, are relatively large, comparable to the resistance to in-plane stretching.[5,13] Second, along the central axis, where the tip is indenting perpendicular to the scroll surface, the stiffness profile $k(x)$ reflects details of the tubular geometry that resulted from the roll-up process.

In order to understand the stiffness variation along the central axis, the concept of the indentation persistence length needs to be introduced. This persistence length characterizes the spatial extent of a small local deformation (see Figure 2c), and its value[31] $l_p \approx 4.4R^{3/2}/t_{eff}^{1/2}$ is the result of balancing out-of-plane bending and in-plane stretching energies inside the rolled-up sheet. In the thin-wall limit $t_{eff} \ll R$, l_p can become larger than the scroll length L, in which case the deformation is global and mostly due to bending. As a result, the stiffness profile $k(x)$ shows a single peak at the center, and a slow monotonic drop-off to either side that arises from nonaffine deformation involving the whole tube length.

As the walls become thicker, stretching starts to contribute significantly and the deformation becomes localized to a finite zone of extent $l_p < L$. Integrating both contributions across the deformation zone and minimizing the total energy results in an x-independent stiffness given by[29]

$$k = 1.18E_{2D}\left(\frac{t_{eff}}{R}\right)^{3/2} \quad (1)$$

In this limit the stiffness depends on the local radius R and the local effective thickness t_{eff}, rather than on the global structure of the scroll. Only once the indenter gets to within l_p from a change in R or t_{eff}, for example, near either end of the tube, does the deformation energy, and thus the stiffness, change.

Based on these considerations, the ratio l_p/L determines the stiffness profile $k(x)$ along the central axis of a tube, while E_{2D} only sets the overall scale. By analyzing experimental stiffness profiles as in Figure 2 and comparing them to finite element simulations of the experimental tube geometries, we can extract information about the persistence length l_p and calculate the effective wall thickness t_{eff}. Given t_{eff}, we then obtain E_{2D} and from it the bending modulus κ.

Finite element simulations of the stiffness profiles were conducted with COMSOL Multiphysics 5.1, using the structural mechanics module. For these simulations, the overall scroll geometry was obtained from SEM or AFM images; the internal scroll geometry, and in particular the local (physical) wall thickness, was reconstructed from models as shown in the Supporting Information. A scroll was then modeled as an axial stack of bonded tube sections of appropriate wall thickness, accounting in cases such as Figure 3d for the fact that an extra (here: third) layer might be present only across a portion of a tube section.

DOI: 10.1021/acs.nanolett.5b02587
Nano Lett. 2015, 15, 6732−6737

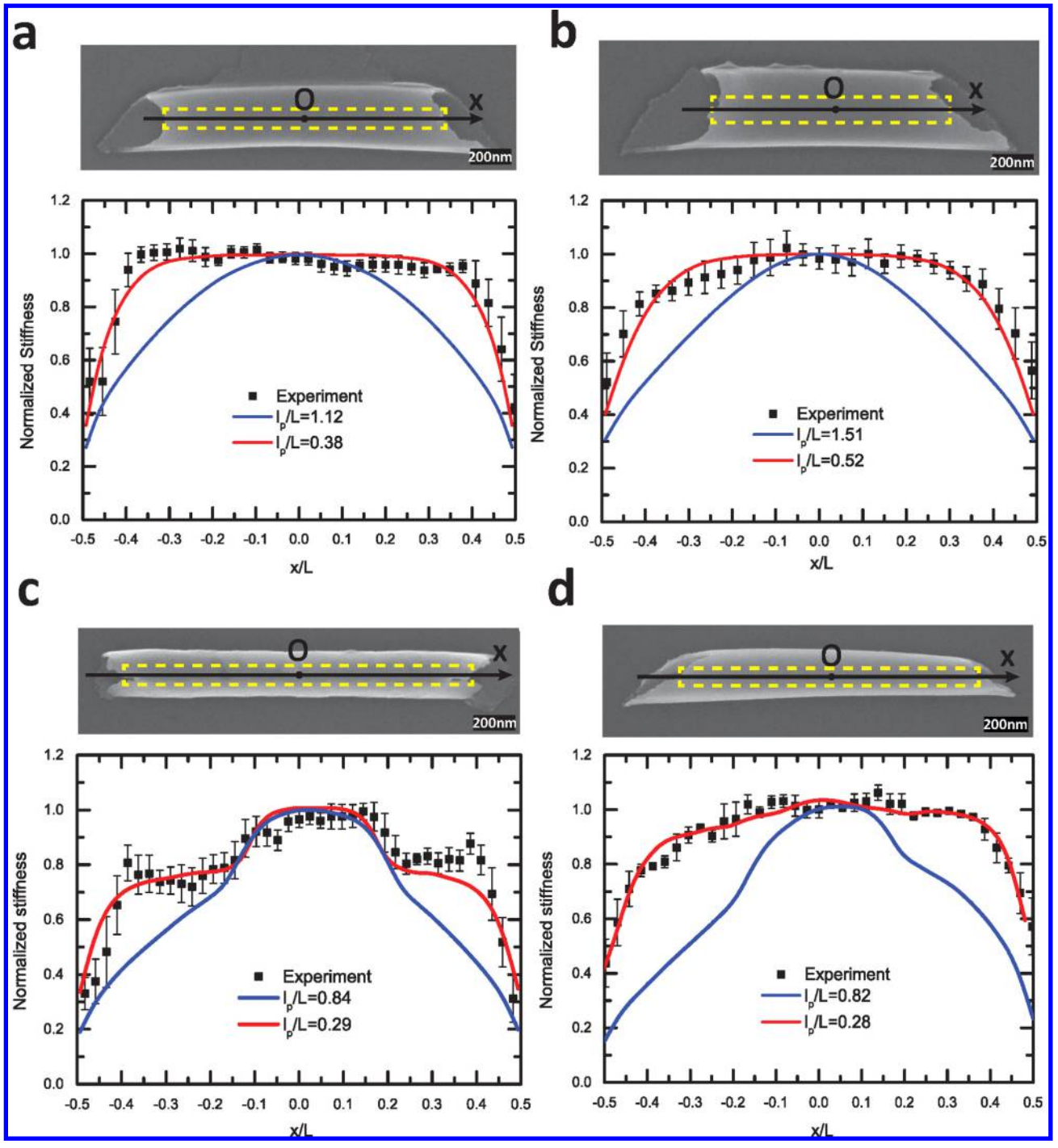

Figure 3. Axial stiffness profiles of scrolls with various geometries. Experimental data are represented by black squares and simulation results by red and blue lines. These profiles contain signatures both of the scroll geometry and of the interplay between resistance to stretching and to bending. The local stiffness of a scroll of length L is normalized by its average value at the center ($x = 0$). The persistence length l_p characterizes the size of the deformation zone due to a local indentation. Four examples are shown of scrolls that differ in l_p/L ratio, shape (cylindrical, conical), and wall thickness. (a) Cylindrical scroll (R = 150 nm, L = 1.39 μm) with uniform wall thickness of 2 monolayers along the top. (b) Cylindrical scroll (R = 180 nm, L = 1.22 μm) with uniform wall thickness of 2 monolayers along the top. (c) Cylindrical scroll (R = 105 nm, L = 1.7 μm) with wall thickness of 2 monolayers at the ends and 3 layers at the center. (d) Cone-shaped scroll (135 nm > R > 80 nm, L = 1.5 μm) with uniform wall thickness of 2 monolayers at the ends and 3 layers at the center. The rectangular frame with the dashed yellow border in the SEM images of the scrolls indicates the area over which the stiffness data were taken and locally averaged. Each data point was averaged among a neighboring 110 × 74 nm area from the stiffness map (see Figure 2e), and the size of the error bars on the plotted experimental data (black squares) correspond to one standard deviation around the mean. Solid curves are finite element simulations for different values of l_p/L, which depends on wall thickness. Using the physical thickness t predicts spatially extended deformation zones and significant end effects (blue) incompatible with the experimental data, which, however, can be reproduced well by assuming a large effective thickness t_{eff} (red). The best-fit ratio $t_{eff}/t \approx 9$ indicates an enhancement of the bending modulus by almost two orders of magnitude over predictions from standard continuum elasticity.

DOI: 10.1021/acs.nanolett.5b02587
Nano Lett. 2015, 15, 6732−6737

From images of individual scrolls together with the associated portions of monolayer that have not curled up, we can find the internal scroll geometry and reconstruct the local wall thickness as a function of axial coordinate x (see Supporting Information Figures S1 and S2). If we use the physical thickness, which is a multiple of the nanoparticle monolayer thickness t_0 = 7 nm, to calculate the persistence length, we find that all nanoscrolls should be within the thin-wall limit, and we would therefore expect that local indentation should lead to global deformation. For example, the scroll shown in Figure 3a has radius R = 150 nm and wall thickness $t = 2t_0$, which gives $l_p \approx 2.1$ μm, larger than the scroll length L = 1.4 μm. The blue trace in that figure shows the corresponding, predicted axial stiffness profile $k(x)$, obtained from the finite element calculation.

The striking discrepancy with the experimental data in Figure 3a demonstrates that nanoparticle scrolls resist indentation as if they had a wall thickness $t_{eff} \gg t$. Best fits of the data to finite element simulations give $l_p/L \approx 0.4$, which implies $t_{eff} \approx 120$ nm or almost 9 times the physical thickness. This large t_{eff} should be viewed as proxy for an unusually large ratio of bending to stretching moduli, i.e., of resistance to bending which far exceeds that expected from a description of the monolayer as homogeneous continuum material.

We find the same qualitative behavior in all nanoparticle scrolls measured. This includes scrolls with larger aspect ratio of R/L (Figure 3b) as well as scrolls with nonuniform wall thickness along their apex (Figure 3c), where the larger stiffness in the center portion arises from the presence of a third layer in the hollow interior underneath the apex (the "lip" portion of the circular sheet at the beginning of the scroll formation). In Figure 3d we show the stiffness profile for a cone-shaped scroll with nonuniform radius along the axis, with higher stiffness toward the smaller radius, in accordance with eq 1. For scrolls in Figure 3a,b, using t_{eff} = 120 nm in the bilayer provides consistently good fits (red traces in Figure 3), while using the physical thickness of 14 nm clearly does not (blue traces).

Note that t_{eff} in this way is extracted from the shape of $k(x)$ alone, independent of the value of E_{2D} (see also Supporting Information Figure S3). The 2D modulus E_{2D} is then found from matching the experimentally measured stiffness in the center of the scroll, $k(0)$, to finite element simulations or, for $l_p \ll L$, directly using eq 1. For scrolls with varying local wall thickness this holds as long as we can assume that the Young's modulus E is independent of wall thickness, so that $E_{2D} = Et$ applies. For our scrolls, t_{eff} and R are of similar magnitude, and thus, via eq 1, the same is true for k and E_{2D}. Indeed, the experimental $k(0)$ values of 10−30 N/m in the central, two-layered scroll sections are reproduced by the simulations with E_{2D} ranging from 34 to 65 N/m. Using t = 14 nm this implies Young's moduli E around 2−4 GPa, fully consistent with prior measurements using stretching.[5,11]

With t_{eff} = 120 nm the bending modulus of a bilayer wall is $\kappa = E_{2D}t_{eff}^2/12(1-\nu^2) \approx 4 \times 10^5$ eV, where we used ν = 0.3 from earlier measurements.[14] This value for κ is about 2 orders of magnitude larger than had we used the physical thickness t, which would give $\kappa_0 \approx 6 \times 10^3$ eV. This breakdown of classical continuum elasticity signals the importance of taking into account the discrete and finite size nature of the constituent units as well as any structural heterogeneity in ultrathin nanoscale systems. Both can result in nonlocal coupling of rotational degrees of freedom.[21−25] We note that the in-plane behavior, and thus E_{2D}, is not affected since no particle rotation is involved during planar stretching. The general result is a correction to the bending modulus given by[21,23]

$$\kappa = \kappa_0\left[1 + 6(1-\nu)\left(\frac{l}{t}\right)^2\right] \quad (2)$$

which can become dominant when t falls below a material-specific length l. For our experiments with bilayer walls, $\kappa/\kappa_0 = (t_{eff}/t)^2 \approx 9^2$ implies $l \approx 60$ nm, a distance of roughly 8−9 particle diameters; l is the length scale at which classical elasticity breaks down for the specific material.[24] In our nanoparticle membranes, we expect l to change with nanoparticle sizes, the type of ligands between particles, and the crystalline grain sizes in the membranes.

An easily testable prediction of eq 2 is that, once $t \ll l$, the effective thickness t_{eff} should stop changing with physical thickness and level off at $t_{eff} \approx 2l$ (see Supporting Information Figure S4). Specifically, eq 2 predicts that going from two-layer (14 nm) to three-layer (21 nm) sections of scrolls as in Figure 3c,d changes t_{eff} by <1%. Simulations based only on the scroll geometry and using the same $E = E_{2D}/t$ and same t_{eff} = 120 nm for both the two- and three-layer sections, with no further adjustable parameters, indeed reproduce the experimental data extremely well (red traces in Figure 3c,d).

These results constitute the first direct measurements of the bending modulus for nanoparticle membranes. While the membranes are obviously quite flexible because they are so thin, their resistance to bending is nevertheless much larger than standard elasticity would predict based on the in-plane stretching behavior. Such remarkably strong enhancement of κ indicates that understanding out-of-plane bending in these systems necessitates new considerations. At this stage, it remains an open question how the large κ/κ_0 ratio arises from nonlocal, ligand-mediated interactions between nanoparticles. In the Supporting Information Figure S5 we show that some aspects related to increasing t_{eff} can be captured by a simplified model. More detailed insights are likely to require extensive molecular dynamics simulations, such as those recently employed to investigate stretching of planar layers.[11] By varying ligand length and nanoparticle shape, it should be possible control t_{eff} and thus tailor κ and E_{2D} independently, an intriguing option for nanomechanical systems. The new method introduced here for obtaining both stretching and bending moduli from a single set of indentation measurements coupled with finite element simulations circumvents the traditional requirement of separate experiments. Since the method is only based on the tube geometry and elastic theory, it should have general applicability across a wide range of materials and size scales, from nano- and microtubules to truly macroscopic objects.

■ ASSOCIATED CONTENT

Supporting Information

The Supporting Information is available free of charge on the ACS Publications website at DOI: 10.1021/acs.nanolett.5b02587.

Paper models of nanoparticle scrolls, finite element simulation results, and simplified models to explain enhanced bending modulus (PDF)

DOI: 10.1021/acs.nanolett.5b02587
Nano Lett. 2015, 15, 6732−6737

AUTHOR INFORMATION

Corresponding Author

*E-mail: yifanw@uchicago.edu.

Notes

The authors declare no competing financial interest.

ACKNOWLEDGMENTS

We thank Ed Barry, Pongsakorn Kanjanaboos, Ivo Peters, Tom Witten, and Qin Xu for many stimulating discussions. The work was supported by the NSF through grants DMR-1207204 and DMR-1508110 and through the Chicago MRSEC under NSF DMR-0820054 and DMR-1420709. Use of the Center for Nanoscale Materials, an Office of Science user facility, was supported by the U.S. Department of Energy, Office of Science, Office of Basic Energy Sciences, under contract no. DE-AC02-06CH11357. J.L. acknowledges fellowship support from the Ministry of Science and Technology, PRC (no. 2011CB933001, 2012CB932702) and the National Natural Science Foundation of China (no. 60971001) and thanks the University of Chicago for its hospitality during his stay there. E.E. acknowledges support from the Simons foundation.

REFERENCES

(1) Bunch, J. S.; Zande, A. M.; Verbridge, S. S.; Frank, I. W.; Tanenbaum, D. M.; Parpia, J. M.; Craighead, H. G.; McEuen, P. L. *Science* **2007**, *315*, 490.

(2) Lee, C.; Wei, X.; Kysar, J. W.; Hone, J. *Science* **2008**, *321*, 385.

(3) Blees, M. K.; Barnard, A. W.; Rose, P. A.; Roberts, S. P.; McGill, K. L.; Huang, P. Y.; Ruyack, A. R.; Kevek, J. W.; Kobrin, B.; Muller, D. A.; McEuen, P. L. *Nature* **2015**, *524*, 204−207.

(4) Lin, Y.; Skaff, H.; Böker, A.; Dinsmore, A. D.; Emrick, T.; Russell, T. P. *J. Am. Chem. Soc.* **2003**, *125*, 12690−12691.

(5) Mueggenburg, K. E.; Lin, X. M.; Goldsmith, R. H.; Jaeger, H. M. *Nat. Mater.* **2007**, *6*, 656−660.

(6) Cheng, W.; Campolongo, M. J.; Cha, J. J.; Tan, S. J.; Umbach, C. C.; Muller, D. A.; Luo, D. *Nat. Mater.* **2009**, *8*, 519−525.

(7) Dong, A.; Chen, J.; Vora, P. M.; Kikkawa, J. M.; Murray, C. B. *Nature* **2010**, *466*, 474−477.

(8) Olichwer, N.; Leib, E. W.; Halfar, A. H.; Petrov, A.; Vossmeyer, T. *ACS Appl. Mater. Interfaces* **2012**, *4*, 6151−6161.

(9) Pham, J. T.; Lawrence, J.; Lee, D. Y.; Grason, G. M.; Emrick, T.; Crosby, A. *Adv. Mater.* **2013**, *25*, 6703−6708.

(10) Rupich, S. M.; Castro, F. C.; Irvine, W. T. M.; Talapin, D. V. *Nat. Commun.* **2014**, *5*, 5045.

(11) Salerno, K. M.; Bolintineanu, D. S.; Lane, J. M. D.; Grest, G. S. *Phys. Rev. Lett.* **2014**, *113*, 258301.

(12) Liao, J.; Blok, S.; Molen, S. J.; Diefenbach, S.; Holleitner, A. W.; Schönenberger, C.; Vladyka, A.; Calame, M. *Chem. Soc. Rev.* **2015**, *44*, 999.

(13) He, J.; Kanjanaboos, P.; Frazer, N. L.; Weis, A.; Lin, X. M.; Jaeger, H. M. *Small* **2010**, *6*, 1449−1456.

(14) Kanjanaboos, P.; Joshi-Imre, A.; Lin, X. M.; Jaeger, H. M. *Nano Lett.* **2011**, *11*, 2567−2571.

(15) Wang, Y.; Kanjanaboos, P.; Barry, E.; Mcbride, S.; Lin, X. M.; Jaeger, H. M. *Nano Lett.* **2014**, *14*, 826−830.

(16) Guo, X.; Li, H.; Ahn, B. Y.; Duoss, E. B.; Hsla, K. J.; Lewis, J. A.; Nuzzo, R. G. *Proc. Natl. Acad. Sci. U. S. A.* **2009**, *106*, 20149−20154.

(17) Chun, I. S.; Challa, A.; Derickson, B.; Hsia, A. J.; Li, X. *Nano Lett.* **2010**, *10*, 3927−3932.

(18) Ionov, L. *Soft Matter* **2011**, *7*, 6786−6791.

(19) Yao, K.; Manjare, M.; Barrett, C. A.; Yang, B.; Salguero, T. T.; Zhao, Y. *J. Phys. Chem. Lett.* **2012**, *3*, 2204−2208.

(20) Nelson, D. R.; Peliti, L. *J. Phys. (Paris)* **1987**, *48*, 1085−1092.

(21) Yang, F.; Chong, A. C. M.; Lam, D. C. C.; Tong, P. *Int. J. Solids Struct.* **2002**, *39*, 2731−2743.

(22) McFarland, A. W.; Colton, J. S. *J. Micromech. Microeng.* **2005**, *15*, 1060−1067.

(23) Park, S. K.; Gao, X. L. *J. Micromech. Microeng.* **2006**, *16*, 2355−2359.

(24) Maranganti, R.; Sharma, P. *Phys. Rev. Lett.* **2007**, *98*, 195504.

(25) Askes, H.; Aifantis, E. C. *Int. J. Solids Struct.* **2011**, *48*, 1962−1990.

(26) Jiang, Z.; He, J.; Deshmukh, S. A.; Kanjanaboos, P.; Kamath, G.; Wang, Y.; Sankaranarayanan, S. K. R. S.; Wang, J.; Jaeger, H. M.; Lin, X. M. *Nat. Mater.* **2015**, *14*, 912.

(27) Wang, Y.; Kanjanaboos, P.; Mcbride, S.; Barry, E.; Lin, X. M.; Jaeger, H. M. *Faraday Discuss.* **2015**, *181*, 325.

(28) Lin, X. M.; Jaeger, H. M.; Sorensen, C. M.; Klabunde, K. J. *J. Phys. Chem. B* **2001**, *105*, 3353−3357.

(29) Pablo, P. J.; Schaap, I. A. T.; Mackintosh, F. C.; Schmidt, C. F. *Phys. Rev. Lett.* **2003**, *91*, 098101.

(30) Schaap, I. A. T.; Carrasco, C.; Pablo, P. J.; MacKintosh, F. C.; Schmidt, C. F. *Biophys. J.* **2006**, *91*, 1521−1531.

(31) Mahadevan, L.; Vaziri, A.; Das, M. *Europhys. Lett.* **2007**, *77*, 40003.

DOI: 10.1021/acs.nanolett.5b02587
Nano Lett. 2015, 15, 6732−6737